International Information and Engineering Technology Association
Advancing the World of Information and Engineering

Ingénierie des Systèmes d'Information
Vol. 31, No. 6, June, 2026, pp. 1915-1925
Journal homepage: http://iieta.org/journals/isi

A Hybrid DTCWT–NSCT Framework for Multimodal Medical Image Fusion and Structural Information Enhancement

Bharati Narute[1,2*], Prashant Bartakke[1]

[1] Department of Electronics and Telecommunication, College of Engineering, Pune 411005, India
[2] Department of Electronics and Telecommunication, M.E.S. Wadia College of Engineering, Pune 411001, India

Corresponding Author Email: bharati.narute@mescoepune.org

https://doi.org/10.18280/isi.310614

Received: 5 January 2026
Revised: 4 March 2026
Accepted: 15 March 2026
Available online: 30 June 2026

Keywords:
multimodal medical image fusion, Dual-Tree Complex Wavelet Transform, Non-Subsampled Contourlet Transform, transform-domain fusion, medical image enhancement, structural information preservation

ABSTRACT

Multimodal medical image fusion plays an important role in integrating complementary anatomical and functional information from different imaging modalities, thereby improving the quality and interpretability of medical image analysis. However, existing fusion approaches often face limitations in preserving fine structural details, maintaining edge continuity, and achieving effective multi-scale representation. This study proposes a hybrid fusion framework based on the Dual-Tree Complex Wavelet Transform (DTCWT) and Non-Subsampled Contourlet Transform (NSCT) for multimodal medical image fusion. The proposed framework combines the directional selectivity and approximate shift invariance of DTCWT with the multi-scale and multi-directional representation capability of NSCT to achieve improved structural and textural information preservation. MRI and Single-Photon Emission Computed Tomography (SPECT) image pairs from a publicly available medical image database were used for experimental evaluation. The proposed method was compared with conventional fusion techniques, including Principal Component Analysis (PCA), Discrete Wavelet Transform (DWT), Pulse-Coupled Neural Network (PCNN), NSCT, Non-Subsampled Shearlet Transform (NSST), and guided filtering-based approaches, using objective evaluation metrics such as Fusion Factor, Image Quality Index, Multi-Scale Structural Similarity Index, Edge Quality Measure, and Peak Signal-to-Noise Ratio. Experimental results demonstrate that the proposed DTCWT–NSCT framework achieves superior fusion performance by preserving complementary modality information, enhancing structural consistency, and reducing information distortion. The proposed method provides an effective transform-domain solution for high-quality multimodal medical image fusion and may support improved visualization in medical image analysis applications.

1. INTRODUCTION

Multimodal medical image fusion integrates complementary information from different imaging modalities to improve diagnostic accuracy. Spatial-domain fusion methods are simple and computationally efficient but often suffer from poor contrast and limited spectral utilization. Consequently, frequency-domain fusion techniques, employing transforms, such as wavelets, curvelets, contourlets and shearlets have gained prominence across fields including signal analysis and image processing. Among these, the Discrete Wavelet Transform (DWT) has been widely used due to its superior spatial-frequency localization, outperforming pyramid-based methods. While wavelet-based fusion has been extensively applied in multi-focus, remote sensing, and infrared imaging, its use in medical imaging remains relatively limited. With the growing availability of diverse imaging modalities, clinicians increasingly rely on fusion techniques to combine anatomical and functional details, offering a more comprehensive view of tissues and organs for effective diagnosis and treatment planning.

2. RELATED WORK

Multimodal medical image fusion has attracted significant research attention, with numerous approaches proposed to improve efficiency, accuracy, and clinical applicability. Early methods primarily focused on transform-domain techniques due to their ability to capture spatial–frequency characteristics effectively. For instance, Kumar [1] introduced a computationally efficient fusion method based on Discrete Cosine Harmonic Wavelet (DCHWT), while Bhatnagar et al. [2] developed a framework utilizing the Non-Subsampled Contourlet Transform (NSCT) to enhance directional representation. Similarly, Singh and Khare [3] proposed a multi-resolution fusion approach using Daubechies Complex Wavelet Transform (DCxWT), and Yang et al. [4] designed a fusion framework for visual sensor networks. Vijayarajan and Muttan [5] and Agarwal and Bedi [6] explored the Principal Component Analysis (PCA) and wavelet-based hybrid methods.

Geng et al. [7] presented a Multi-Non-Subsampled Directional Filter Bank transform, integrating multiwavelet and NSDFB through the Discrete Fractional Wavelet Transform (DFRWT), while Xu et al. [8] applied a weighted regional variance method to combine coefficients across subbands. Karthikeyan and Ramadoss [9] introduced a fusion strategy based on Dual-Tree Complex Wavelet Transform (DTCWT) and Self-Organizing Feature Maps (SOFM). Similarly, Chavan et al. [10] utilized an NSRCxWT-based approach for medical data integration. Hill et al. [11] applied perceptual models such as luminance and contrast masking for perceptual image fusion. El-Hoseny et al. [12] conducted a comparative analysis of fusion techniques, outlining their advantages and limitations. Udhaya Suriya and Rangarajan [13] demonstrated a multimodal fusion method for brain tumor diagnosis using Magnetic Resonance Imaging (MRI) and Positron Emission Tomography (PET) scans, while Kaur et al. [14] proposed a multi-resolution framework employing stationary wavelets with coefficient spreading.

Further, Bhateja et al. [15] designed a two-stage cascading fusion framework combining SWT and NSCT for Magnetic Resonance Imaging–contourlet transform (MRI–CT) images, whereas Gomathi and Kalaavathi [16] presented NSCT-based methods for multi-input image integration. Moin et al. [17] developed a weighted PCA-contourlet method, and Luo et al. [18] proposed a contextually aware multimodal fusion model. Mehta and Budhiraja [19] and Wang [20] advanced hybrid techniques combining wavelet decomposition, NSCT, and SR-based fusion strategies. Rajalingam et al. [21] contributed several hybrid methods, including DFRWT–NSCT frameworks and a deep learning method [22], with applications in pathology detection (e.g., neurocysticercosis, degenerative diseases, and neoplasms). Pei et al. [23] presented a two-scale multimodal medical image framework using guided filtering and sparse representation.

To enhance spatial consistency, Li et al. [24] introduced a guided filtering-based weighted average method, while Liu et al. [25, 26] proposed shearlet-guided and probabilistic neural network-based fusion algorithms, both demonstrating superior subjective and objective results on CT and MRI datasets. Du et al. [27], provided a comprehensive review of medical fusion methodologies, highlighting the key scientific challenges in multimodal fusion. Similarly, Yang et al. [28] presented a gradient-domain-driven method, and Jian et al. [29] proposed a hybrid bilateral–rolling guidance filter approach for artifact reduction. Zhu et al. [30] developed a Hybrid Multiscale Decomposition method (HMSD-GDGF), combining multiscale decomposition and guided filtering.

Sreeja and Hariharan [31] suggested edge- and texture-enhanced fusion methods for liver and abdominal imaging, while Na et al. [32] proposed a guided-filter (GF)-based DWT framework for CT–MRI fusion, enhancing contour preservation and radiation protection. Meher et al. [33] reviewed regional fusion methods with detailed evaluation metrics, and Daniel et al. [34, 35] introduced optimization-driven homomorphic wavelet and spectrum mask fusion approaches using hybrid Genetic–Grey Wolf and OSMF techniques. El-Hoseny et al. [36] proposed a DTCWT fusion system optimized with a Modified Central Force Optimization method, while Singh and Singh [37] designed a hybrid PSO–GWO algorithm to balance convergence, stability, and exploration-exploitation trade-offs.

From the reviewed literature, it is evident that multimodal medical image fusion has evolved from conventional transform-based methods (e.g., DWT and PCA) to advanced hybrid, filtering-based, and optimization-driven frameworks. Although NSCT and DTCWT provide improved multi-scale and directional representations, existing methods still face several challenges, including high computational complexity, insufficient preservation of fine details, and limited balance between global structure and local feature representation. Furthermore, many recent approaches rely on complex optimization or learning-based strategies, which may reduce interpretability and increase dependency on parameter tuning or training data. Therefore, there remains a need for a computationally efficient, interpretable, and robust fusion framework that effectively integrates complementary strengths of existing transforms. Motivated by these limitations, the present study proposes a hybrid DTCWT–NSCT-based fusion approach, aiming to achieve improved structural preservation, enhanced directional representation, and balanced integration of global and local image features for reliable clinical interpretation. This paper is organized as follows: Section 2 presents a detailed review of the relevant literature. Section 3 provides a brief introduction to the theoretical background of DTCWT and NSCT. Section 4 describes the proposed Hybrid Fusion approach based on the Dual-Tree Complex Wavelet Transform–Non-Subsampled Contourlet Transform (DTCWT–NSCT) algorithm. Section 5 discusses the experimental results and their implications. Finally, Section 6 concludes the paper with key findings and future research directions.

3. PROPOSED METHODOLOGY

3.1 Dual Tree Complex Wavelet Transform

Kingsbury's and Selesnick's DTCWT forms the basis of the Redundant Complex Wavelet Transform (RCWT). In the DTCWT framework, two parallel DWT filter bank trees operate simultaneously to generate complex-valued coefficients. Figures 1 and 2 illustrate the analysis and synthesis filter bank structures used in this approach. In this formulation, the conventional real-valued filters of a standard DWT are extended to approximate analytic filters, resulting in a dual-tree structure. This structure consists of two parallel filter banks: the first tree employs real-valued filters, while the second tree uses filters designed to approximate the Hilbert transform of the first, thereby producing the imaginary components required for complex representation. This dual-tree configuration enables improved directional selectivity and approximate shift invariance compared to traditional DWT. Figures 1 and 2 present three levels of decomposition for one-dimensional analysis and synthesis filter banks. Conceptually, the DTCWT can be interpreted as two coordinated DWT decompositions operating in parallel, whose outputs are combined to form complex coefficients. The first tree is a real one, while the other is a work of fiction. Complex filters in 1D DTCWTare indicated as $(h_x j g_x)$. Here h_x is the set of filters $\{h_0, h_1\}$, and g_x is the set of filters $\{g_0, g_1\}$.

The low-pass filter h_0, h_1 is for actual trees, while the high-pass filter g_0, g_1 is for imagined trees; both use real values. The numerical values of the filter coefficients h_0 and h_1 at the first and subsequent levels are distinct.

Orthogonal or bi-orthogonal pairings can be seen in Figure 1 between the pairs of analysis filtersand the synthesis filter pairs. The 2D DTCWT structure is a two-dimensional enlargement ofconjugate filtering. Figure 3 depicts the 2D Dual Tree filter bank layout.

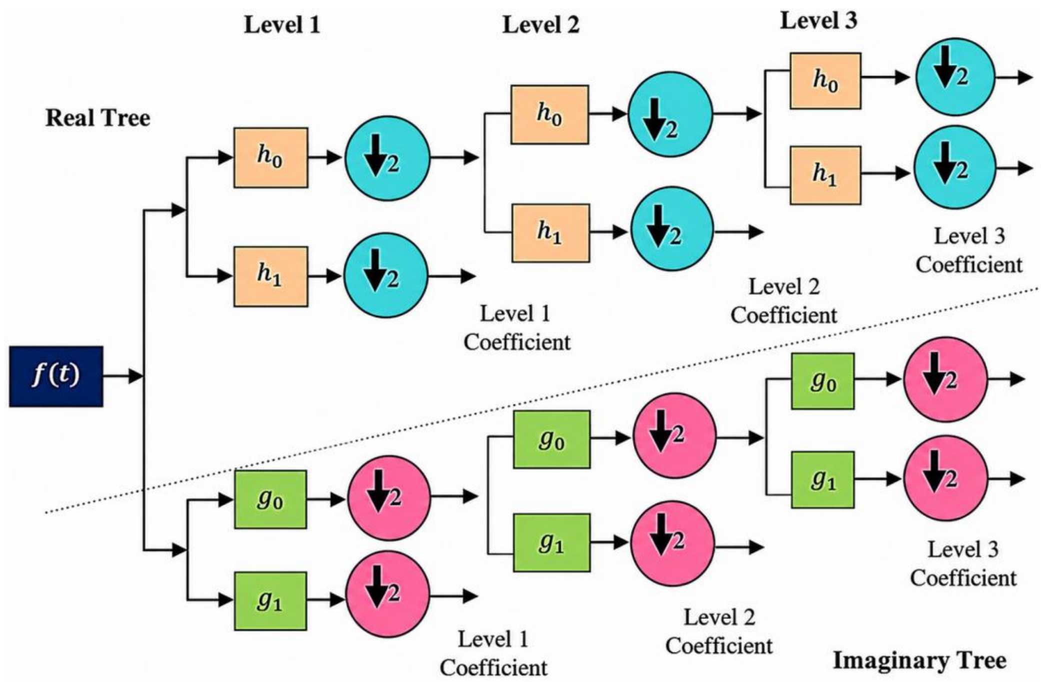

Figure 1. Analysis filter bank for 1D Dual-Tree Complex Wavelet Transform (DTCWT)

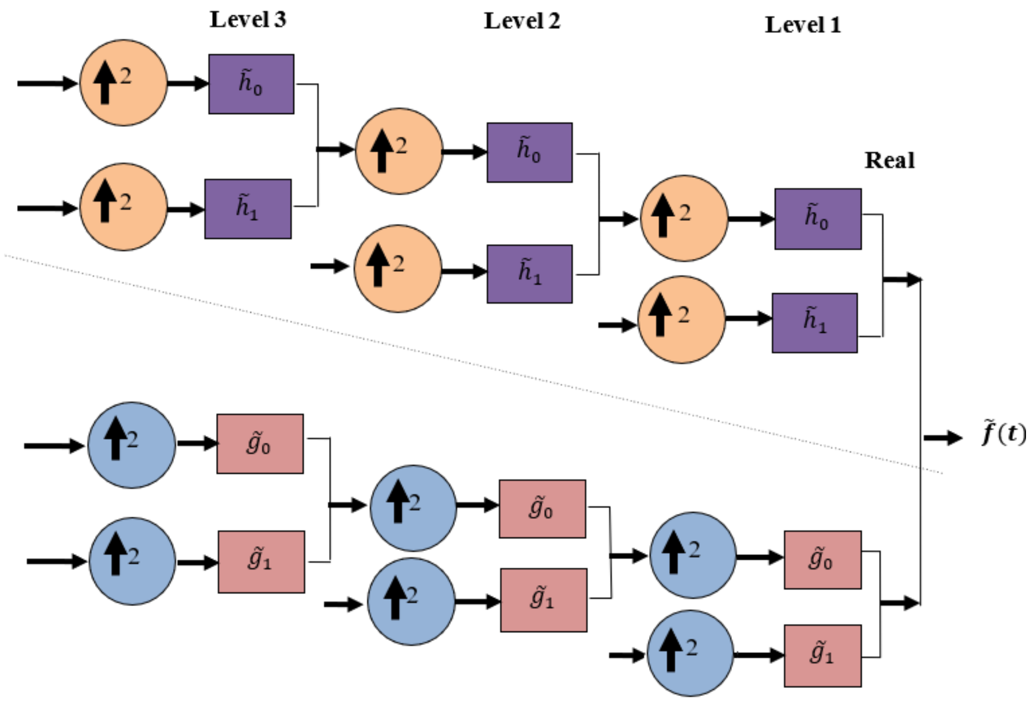

Figure 2. Synthesis filter bank for 1D Dual-Tree Complex Wavelet Transform (DTCWT)

For a 2D structure, four trees are required for analysis and synthesis. For two dimensions, the conjugate filter pairs are:

$$(h_x + jg_x)(h_y + jg_y) = (h_x h_y - g_x g_y) + j(h_x g_y + g_x h_y) \quad (1)$$

Figure 3 illustrates the 2D dual-tree filter bank structure, where the real and imaginary components are generated through coordinated filtering operations. This configuration allows the DTCWT to capture image features along multiple orientations more effectively than conventional wavelet transforms.

3.1.1 Traits of a Dual-Tree Complex Wavelet Transform

•Provides approximate shift invariance, ensuring robustness to small spatial translations.

•Offers enhanced directional selectivity with six distinct orientations in 2D.

•There is no aliasing in DTCWT, hence there are no signal artifacts.

•Improves representation of edge singularities and geometric features.

•Reduces aliasing artifacts compared to standard DWT.

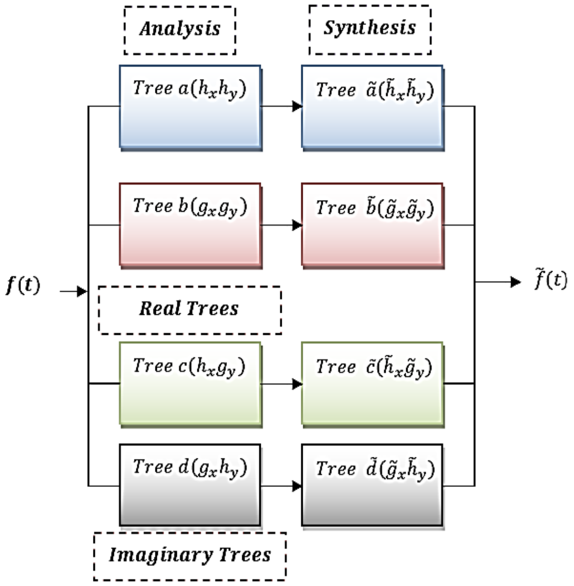

Figure 3. Structure of 2D Dual-Tree Complex Wavelet Transform (DTCWT) filter bank

3.2 Non-Subsampled Contourlet Transform

The NSCT is an advanced multi-resolution and multi-directional image representation technique developed to overcome the limitations of traditional wavelet transforms. Unlike DWT, which provides limited directional information, the CT enables efficient representation of smooth contours and edges across multiple directions and scales. The contourlet transform achieves this through a combination of a Laplacian Pyramid (LP) for multi-scale decomposition and a Directional Filter Bank (DFB) for capturing directional information. However, the use of downsampling and upsampling operations in the original contourlet framework introduces shift variance and may lead to pseudo-Gibbs artifacts near singularities. Therefore, the NSCT is superior at fusing images.

Smooth contours can be described using a method called "contouring," which accomplishes a sparse expansion by using square-shaped brush strokes and many fine "dots" to get over the restrictions imposed by wavelet. By combining the LP with the DFB, Contourlet is able to do multi-scale and directed decomposition. When compared to wavelet, there is no limit to the possible number of level-by-level direction decompositions. The quality of the original contourlet is degraded by LP and DFB downsamplers and upsamplers. Pseudo-Gibbs events are localized around singularities due to the lack of shift invariance. NSCT gets rid of downsamplers and upsamplers during an image's decomposition and reconstruction processes.

To get around wavelet's restrictions, contourlet—a method for depicting smooth contours—uses square-shaped brush strokes and a lot of tiny "dots" to create a sparse expansion. Contourlet employs the LP and the DFB to do directed decomposition and multi-scale analysis. Unlike wavelet, there is no limit to the number of potential direction decompositions at any given level. It is unfortunate that the original contourlet has up-samplers and down-samplers in LP and DFB. Due to its lack of shift invariance, pseudo-Gibbs events manifest themselves in the vicinity of singularities. When an image is decomposing or being reconstructed using NSCT (Figure 4), down-samplers and up-samplers are eliminated.

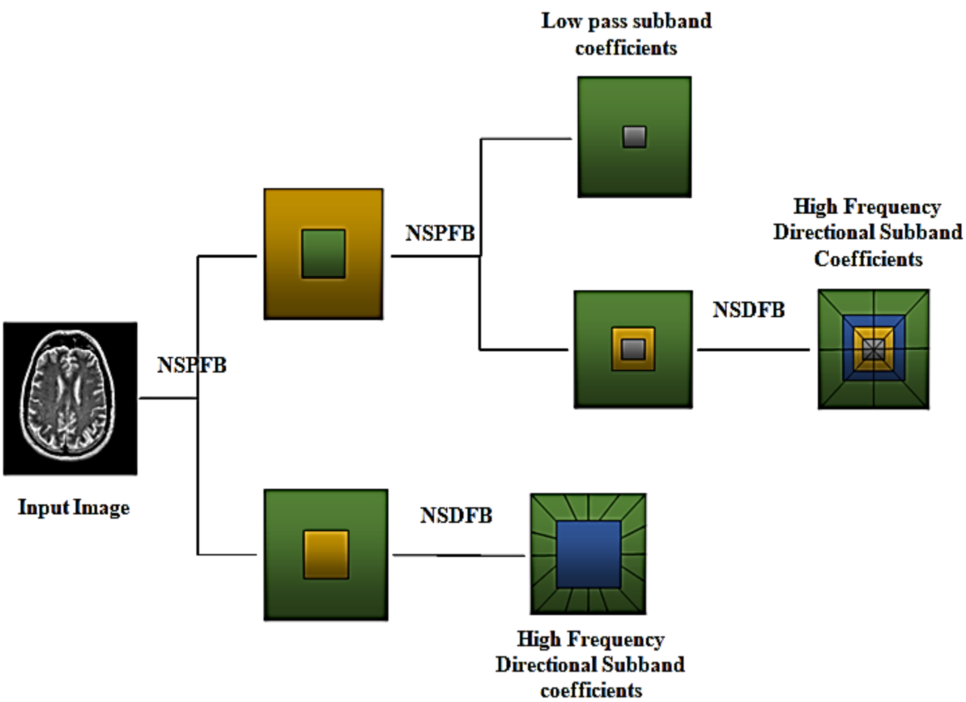

Figure 4. Non-Subsampled Contourlet Transform (NSCT) decomposition framework

4. ALGORITHM FOR HYBRID FUSION PROPOSED (DTCWT-NSCT)

Spatial domain, transform domain, and other constraints of conventional image fusion techniques a innovative method for merging several images is presented in this research it makes use of fuzzy logic and neural network methods. In this method, NSCT and DTCWT are combined. The optimal fusion approach (DTCWT-NSCT) is depicted in block form in Figure 5.

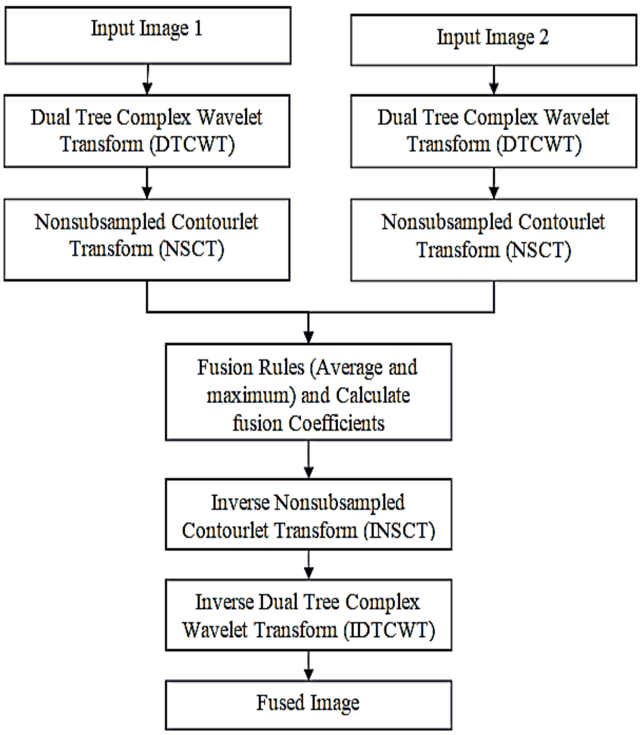

Figure 5. The proposed hybrid fusion algorithm is depicted as a block diagram (DTCWT-NSCT)

4.1 Using Non-Subsampled Contourlet Transform to reconstruct the Dual-Tree Complex Wavelet Transform decomposed image

Since the human visual system is not particularly attuned to specific pixels but rather to information about the image's edges, directions, and textures, implementing the fusion rules of maximum and average to select coefficients produces satisfactory fusion results in the transform domain image fusion. However, computation is time-consuming due to complex limits on high sub-band fusion. Non-Subsampled Shearlet Transform (NSST)-DTCWT is superior at deciphering the basic structure and texturing of medical images since it contains more low-frequency sub-band coefficients. *i* represents the combined image from an MRI and a Single-Photon Emission Computed Tomography (SPECT) scan. First, use the NSCT-DTCWT to derive decomposition coefficients for pictures X and Y. In order to produce high-quality fusion images, optimize the coefficients' absolute values.

Coefficients with lower frequencies are fused using the average fusion rule, whereas those with higher frequencies are fused using the maximum fusion rule. The following are the formulas for average and maximum fusion:

Two fusion rules are described: the median rule (Eq. (3)) and the maximum rule (Eq. (2)).

$$C_{F=}\begin{cases} C_i^1, if\ C_i^1 > C_i^2 \\ C_i^2, if\ C_i^1 < C_i^2 \end{cases} \tag{2}$$

$$C_F = \frac{1}{2}(C_i^1 + C_i^2) \tag{3}$$

where, C_1 and C_2 are the X and Y coefficients of the input image, respectively, and C_F represents the total coefficient. The whole image is reconstructed using the fused coefficients, which are calculated using inverse NSCT and inverse DTCWT CF.

4.2 Steps of the proposed hybrid fusion algorithm

The first step to analyze the two input pictures (labelled *A* and B). Second, send in pictures that have been reduced in size to 256 × 256 pixels. Finally, use the dual tree complex wavelet transform to separate pictures into their corresponding complex coefficients. For each level of decomposition for each of the input images, separate thresholds are determined for both sets of coefficients. In the fourth step, source pictures *A* and *B* are separated into high-frequency sub-bands and a low-frequency sub-bands for each level *k* and direction *l* using the NSCT: A:{H^A, L^A} and M:{H^B, L^B}.

4.2.1 Rule for combining high-frequency parts of an image

Details like edges, textures, and area borders are typically represented in the NSCT transformation's high-frequency sub-pictures. As of recently, the maximal absolute fusion rule has gained a lot of attraction in the high-frequency area. This technique disregards the correlation between adjacent pixels, making it vulnerable to noise that could be misinterpreted as essential information in the final image.

$$X = \begin{Bmatrix} (x,y) | \mu_L^{l,k,l}(x,y) < 0.5 < \mu_H^{l,k,l}(x,y) \\ x = 0,1,\dots M-1, y = 0,1,\dots N-1 \end{Bmatrix} \tag{4}$$

$$H_{k,l}^F(i,j) = \begin{cases} H_{k,l}^A(i,j), & E_{k,l}^E(i,j) \geq E_{k,l}^E(i,j) \\ H_{k,l}^B(i,j), & otherwise \end{cases} \tag{5}$$

4.2.2 Sub-image fusion at low frequencies

In place of the actual source images, which contain most of the energy, the approximation is based on the coefficients found in the low-frequency sub-images. The most efficient method for making the composite bands is to use standard averaging processes. Unfortunately, the merged images lose contrast; therefore, this method can't produce a fused low-frequency component for accurate medical imaging. Variations between neighbouring pixel clusters are more noticeable to the human visual system (HVS) than variations between individual pixels. We employ the Local Energy (LE) to develop fusion rules that enhance the local aspects of the matched image. Our definition of the *LE* is as follows:

$$LE^l\left(L^l(i,j)\right) = \frac{1}{MN}\sum_{m-1}^{M}\sum_{n-1}^{N} L^1\,(i+m, j+n)^2 \tag{6}$$

where, (*M*, *N*) represents the size of the window and (*i*, *j*) represents the low-frequency coefficient's placement in the sub-band. The low-frequency fusion coefficient $L^F(i, j)$ thus conforms to the fusion rule:

$$L^F(i,j) = \begin{cases} L^M(i,j) & LE^M(i,j) > LE^N(i,j) \\ L^N(i,j) & LE^M(i,j) > LE^N(i,j) \\ \dfrac{(L^M(i,j) + L^N(i,j)}{2} & otherwise \end{cases} \tag{7}$$

It is possible to apply fusion rules to make sure that low-frequency coefficients use average fusion and high-frequency coefficients maximize fusion. For the final suggested fused image, apply the IDTCWT inverse transform on the fused image.

5. RESULTS AND DISCUSSION

To determine if the HMMIF Method is effective, MRI, CT, PET, and SPECT scans are being performed on patients suffering from neurocysticercosis, degenerative brain diseases, and neoplastic brain disorders. Due to physical and functional similarities, the subject of input photos for all three categories of medical images is the same. Figures 6–8 display the outcomes of the suggested hybrid image fusion approaches as well as comparisons to counterpart methods. The images are derived from three separate MRI/SPECT scans. All three input images showed the impact of metastatic bronchogenic carcinoma on brain imaging when MRI and SPECT were used together.

5.1 Dataset description

When it comes to healthcare data, images are both the most abundant and most difficult to analyze. Clinicians today frequently perform self-examinations and rely heavily on the interpretation of medical images by overburdened radiologists. This method is checked against a public database available through the Harvard Medical School's online portal [24]. We used data from a database that included 40 individuals' brain MRI and SPECT images. The input size for all images is 356 × 356 pixels. The suggested fusion algorithm is tested against several benchmarks and assessed based on the results. The quality is measured and compared to several standard fusion techniques. This multi-modality medical fusion imaging system is evaluated using the following subjective and objective parameters.

5.1.1 Fusion Factor

It can be used to determine how closely two photos are related after being fused. It takes a stab at estimating how much can be learned from the merged images. (8). The MI_A, MI_B in Eq. (9) represents the mutual information between images A and B. $p(.)$ represents the probability density function. A high Fusion Factor ($FusFac$) means a better-quality fused image was created.

$$FusFac = MI_A + MI_B \tag{8}$$

5.1.2 Image Quality Index

It was first proposed by Xu et al. [8] to compare the original and blended image quality. The Image Quality Index (IQI) is calculated using Eq. (9). Mean and standard deviation are utilized in this formula. The quality of the merged images can be best represented by an IQI score close to one.

$$IQI(A,B) = \frac{2\sigma_{A,B} \,.\, 2\mu_A\mu_B}{(\sigma_A^2 + \sigma_B^2)(\mu_A^2 + \mu_B^2)} \tag{9}$$

5.1.3 Edge Quality Measure

In medical picture analysis, the edges are crucial. To create a fused image, the suggested approach employs edge-related features. Edge quality preservation is predicted using the Edge Quality Measure (EQM) fusion metric. Edge quality is quantified through Eqs. (10)–(12), respectively, are used to estimate EI (edge index) and S_{xy} (window).

$$IQI(A,B) = \frac{2\sigma_{A,B}.\, 2\mu_A\mu_B}{(\sigma_A^2 + \sigma_B^2)(\mu_A^2 + \mu_B^2)} \tag{10}$$

$$EI = \sum_{x=0}^{N-1}\sum_{y=0}^{M-1}(EQ_{a,f}\,(x,y)w_a + EQ_{b,f}\,(x,y)w_b) \tag{11}$$

$$S_{xy} = \sum_{i=0}^{N-1}\sum_{j=0}^{M-1}(W_a(i,j) + W_b(i,j)) \tag{12}$$

5.1.4 Multi-Scale Structural Similarity Index

The mSSIM parameter reveals how structurally comparable the fused picture and source images are Eq. (13) and Eq. (14) are used to calculate the mSSIM (15). Standard deviation = m, mean intensity = m. C_1 = 6:50 and C_2 = 58:52 are fixed values used in each iteration. If mSSIM approaches value one, the similarities are preserved in the fused pictures.

$$SSIM(i,j) = \frac{(2\mu_i\mu_j + C_1)(2\sigma_i\sigma_j + C_2)}{(\mu^2 i + \mu^2 j + C_1)(\sigma^2 i + \sigma^2 j + C_2)} \tag{13}$$

$$mSSIM(i,j) = \frac{1}{M}\sum_{k=1}^{M} SSIM(i_k, j_k) \tag{14}$$

5.1.5 Peak Signal-to-Noise Ratio

This is a numeric estimate. Root Mean Square Error is used to determine it.

$$PSNR = 10 * \log\left(\frac{(f_{max})^2}{RSME^2}\right) \tag{15}$$

where, $f_{\max}$ is the grey level value of the pixel that is the darkest in the reconstructed image. The three sets of MRI and SPECT input images correspond to cases of metastatic bronchogenic carcinoma. Representative pairs of input images are illustrated in Figures 6–8. Conventional fusion approaches applied to these datasets are shown in Figures 6–8(c) through Figures 6–8(h), whereas the fused outputs generated by the proposed method are presented in Figures 6–8(i). To systematically assess the performance of the proposed fusion technique, a comparative evaluation against state-of-the-art methods was conducted, with the corresponding results summarized in Table 1.

Five objective performance metrics were employed in this study, namely FusFac, IQI, EQM, mSSIM, and PSNR. The experimental findings clearly demonstrate that the proposed method consistently outperforms existing approaches across all evaluation criteria. Specifically, the results in Table 1 reveal the following key observations:

- The proposed fusion method achieves the highest performance values in all five metrics—FusFac, IQI, mSSIM, EQM, and PSNR—when compared to conventional methods.
- The superiority of the proposed approach is particularly evident in terms of FusFac and IQI, highlighting its ability to preserve complementary information from the source modalities while enhancing the overall perceptual quality of the fused image.

In summary, the results validate the effectiveness of the proposed fusion framework, establishing it as a robust and superior alternative to conventional image fusion techniques for medical imaging applications involving metastatic bronchogenic carcinoma.

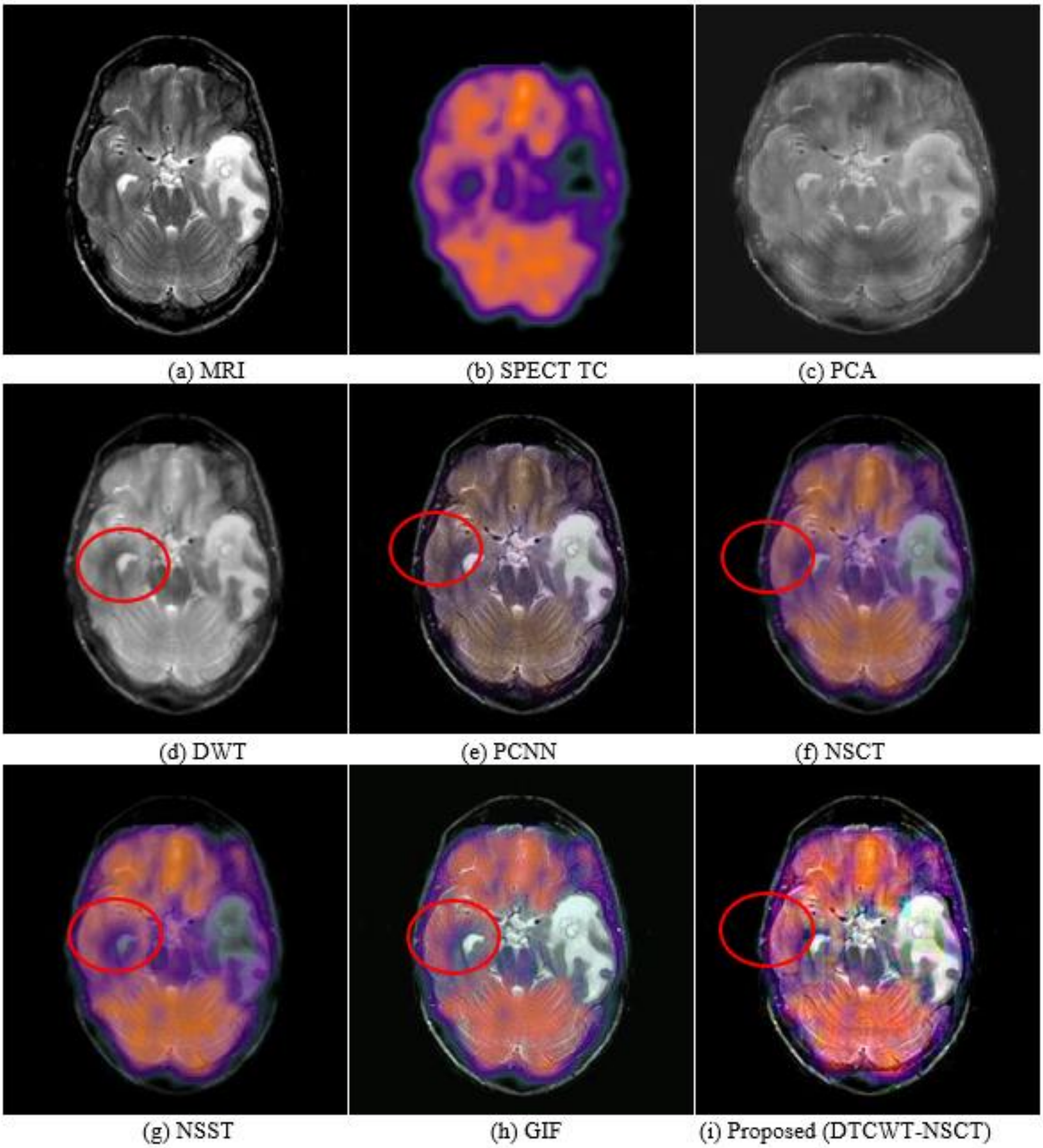

Figure 6. Input Magnetic Resonance Imaging (MRI) and Single-Photon Emission Computed Tomography (SPECT) images used for fusion experiments (Set 1)

Table 1. Comparison of performance measures for three distinct fusion methods

Study Set	Metrics Method	FusFac	IQI	mSSIM	EQM	PSNR
Pair 1	PCA	2.062	0.451	0.418	0.510	19.02
	DWT	2.571	0.454	0.482	0.517	20.30
	DTCWT	2.671	0.518	0.489	0.529	23.67
	NSCT	2.712	0.534	0.505	0.564	25.30
	NSST	3.011	0.507	0.524	0.557	26.80
	GIF	4.851	0.712	0.792	0.878	34.09
	Proposed Method (DTCWT-NSST)	5.012	0.837	0.871	0.941	35.07
Pair 2	PCA	1.154	0.462	0.423	0.451	29.05
	DWT	2.265	0.558	0.548	0.508	32.39
	GIF	2.412	0.542	0.595	0.549	35.55
	PCNN	2.531	0.528	0.575	0.592	37.40
	NSCT	3.612	0.701	0.670	0.722	39.58

	GIF	4.142	0.920	0.941	0.898	46.62
	Proposed Method (DTCWT-NSST)	4.020	0.940	0.939	0.930	45.72
Pair 3	PCA	1.316	0.498	0.452	0.719	30.12
	DWT	2.362	0.511	0.502	0.728	33.50
	PCNN	2.712	0.532	0.629	0.767	32.65
	NSCT	2.862	0.582	0.635	0.801	34.67
	NSST	3.298	0.682	0.699	0.837	39.43
	GIF	4.701	0.891	0.942	0.942	48.56
	Proposed Method (DTCWT-NSST)	4.804	0.985	0.923	0.421	47.50

Note: PCA = Principal Component Analysis; DWT = Discrete Wavelet Transform; DTCWT = Dual-Tree Complex Wavelet Transform; NSCT = Non-Subsampled Contourlet Transform; NSST = Non-Subsampled Shearlet Transform; PCNN = Pulse-Coupled Neural Network; FusFac = Fusion Factor; IQI = Image Quality Index; mSSIM = Multi-Scale Structural Similarity Index; EQM = Edge Quality Measure; PSNR = Peak Signal-to-Noise Ratio; GIF = Guided Image Fusion.

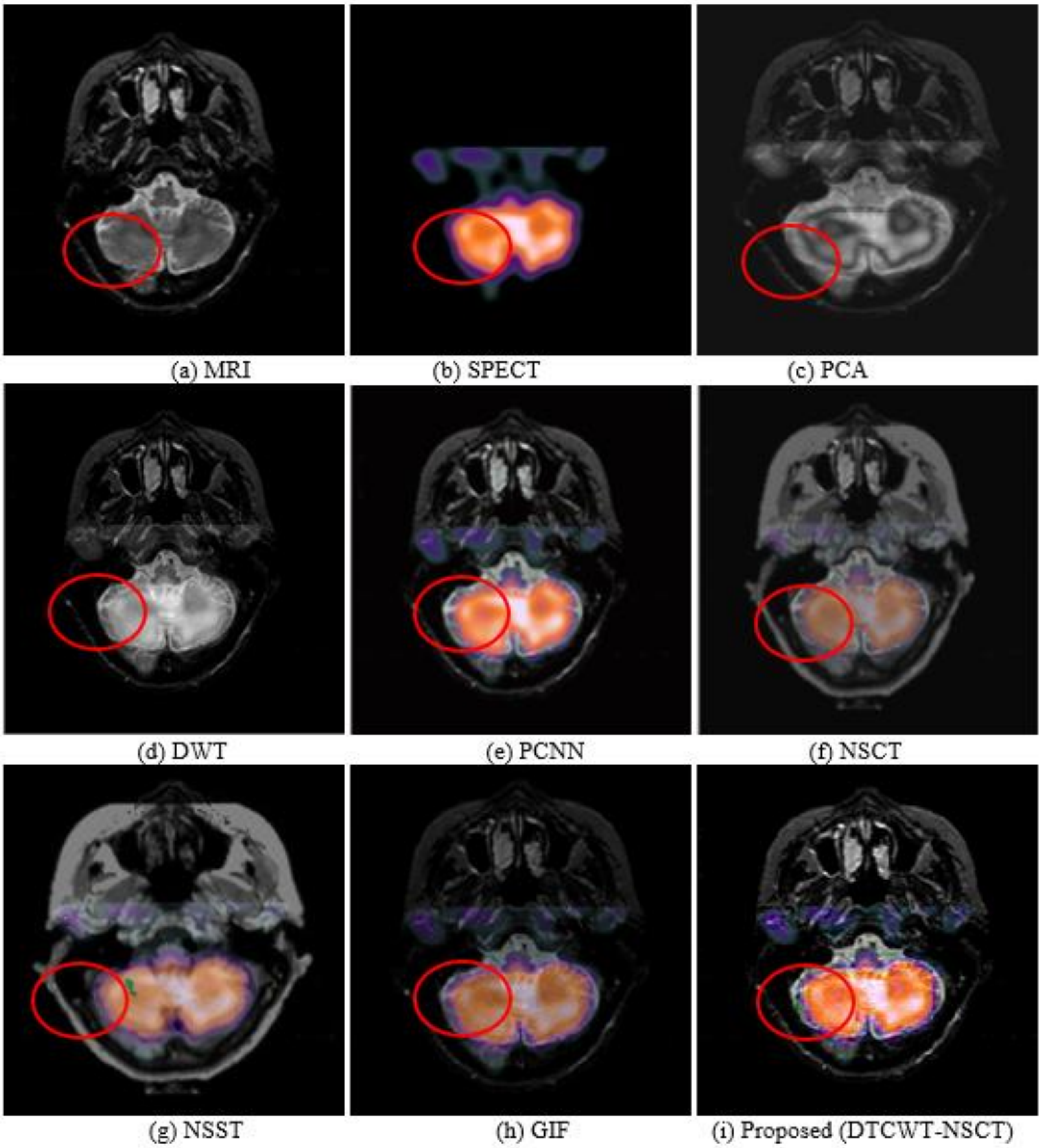

Figure 7. Dual-Tree Complex Wavelet Transform (DTCWT) and Non-Subsampled Contourlet Transform (NSCT) decomposition results for Magnetic Resonance Imaging (MRI) and Single-Photon Emission Computed Tomography (SPECT) images (Set 2)

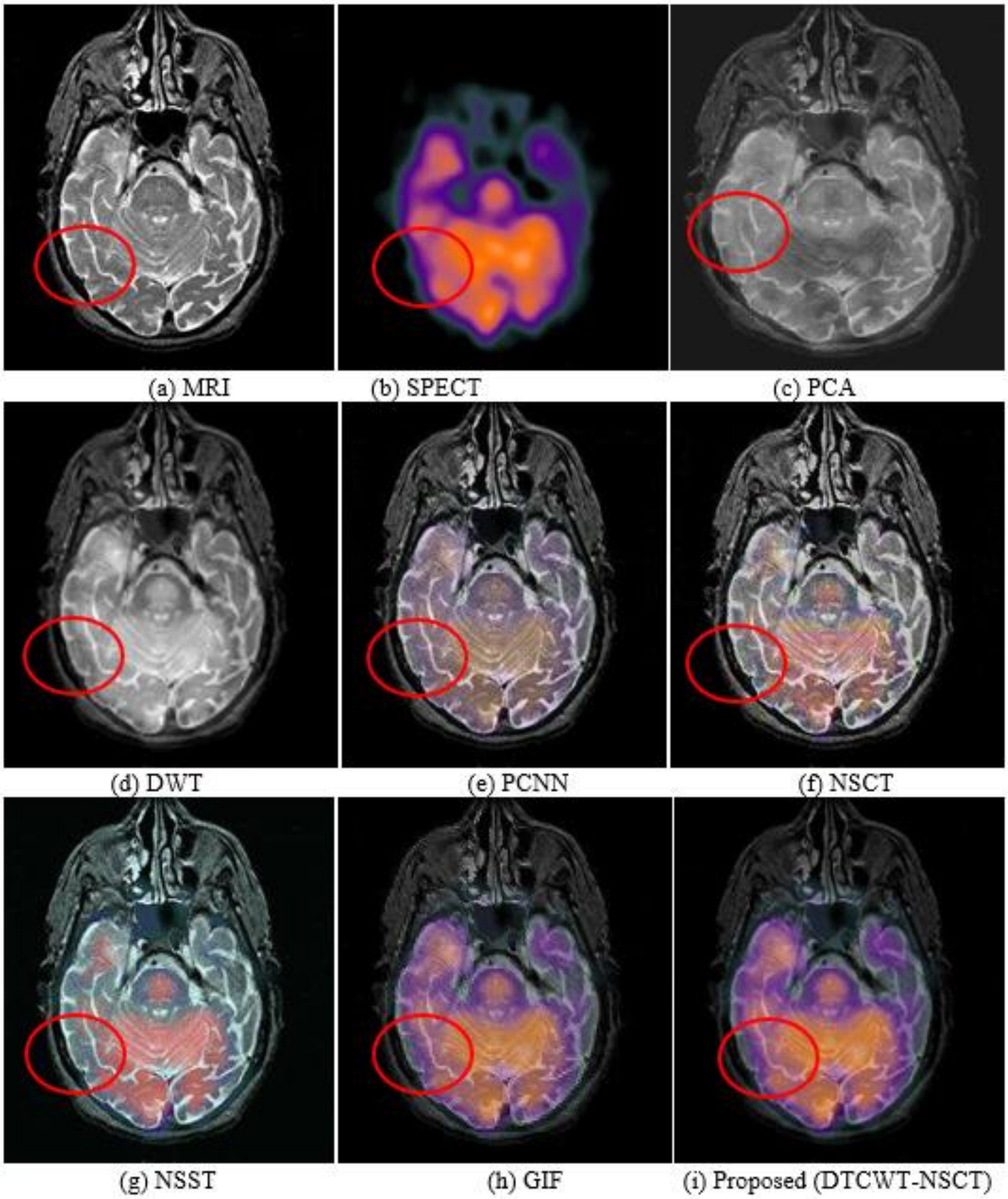

Figure 8. Fused outputs obtained using PCA, DWT, DTCWT, NSCT, NSST, GIF, PCNN, and the proposed DTCWT–NSCT method (Set 3)

Note: PCA = Principal Component Analysis; DWT = Discrete Wavelet Transform; DTCWT = Dual-Tree Complex Wavelet Transform; NSCT = Non-Subsampled Contourlet Transform; NSST = Non-Subsampled Shearlet Transform; GIF = Guided Image Fusion; PCNN = Pulse-Coupled Neural Network.

6. CONCLUSIONS

In this study, a hybrid DTCWT–NSCT framework was developed for multimodal medical image fusion. The proposed method was systematically evaluated using multiple MRI and SPECT image datasets, enabling a comprehensive comparison with conventional fusion techniques.

The performance of the proposed approach was assessed using widely accepted objective metrics, including FusFac, IQI, mSSIM, EQM, Mutual Information (MI), and PSNR. The experimental results demonstrate that the proposed hybrid method effectively preserves and integrates complementary information from different imaging modalities.

Specifically, the method achieves higher FusFac and IQI values, indicating improved information retention and perceptual quality. Enhanced mSSIM and EQM scores confirm superior structural consistency and edge preservation, while increased PSNR and MI values reflect reduced distortion and more effective transfer of modality-specific features.

Overall, the findings confirm that the DTCWT–NSCT-based hybrid framework consistently outperforms conventional fusion approaches across all evaluation metrics. This establishes its effectiveness as a robust and reliable solution for multimodal medical image fusion, particularly in applications requiring accurate integration of anatomical and functional information for clinical decision support.

DATA AVAILABILITY

The datasets analyzed during this study are available in the public resources via http://www.med.harvard.edu/AANLIB/.

REFERENCES

[1] Kumar, B.K.S. (2012). Multifocus and multispectral image fusion based on pixel significance using discrete cosine harmonic wavelet transform. Signal, Image and Video Processing, 7: 1125-1143. https://doi.org/10.1007/s11760-012-0361-x

[2] Bhatnagar, G., Wu, Q.M.J., Liu, Z. (2013). Directive contrast based multimodal medical image fusion in NSCT domain. IEEE Transactions on Multimedia, 15(5): 1014-1024. https://doi.org/10.1109/tmm.2013.2244870

[3] Singh, R., Khare, A. (2014). Fusion of multimodal medical images using Daubechies complex wavelet transform – A multi resolution approach. Information Fusion, 19: 49-60. https://doi.org/10.1016/j.inffus.2012.09.005

[4] Yang, Y., Tong, S., Huang, S.Y., Lin, P. (2014). Dual-tree complex wavelet transform and image block residual-based multi-focus image fusion in visual sensor networks. Sensors, 14(12): 22408-22430. https://doi.org/10.3390/s141222408

[5] Vijayarajana, R., Muttan, S. (2015). Discrete wavelet transform based principal component averaging fusion for medical images. International Journal of Electronics and Communications (AEU), 69(6): 896-902. https://doi.org/10.1016/j.aeue.2015.02.007

[6] Agarwal, J., Bedi, S.S. (2015). Implementation of hybrid image fusion technique for feature enhancement in medical diagnosis. Human-centric Computing and Information Sciences, 5: 3. https://doi.org/10.1186/s13673-014-0020-z

[7] Geng, P., Su, X., Xu, T., Liu, J.S. (2015). Multi-modal medical image fusion based on the multiwavelet and nonsubsampled direction filter bank. International Journal of Signal Processing, Image Processing and Pattern Recognition, 8(11): 75-84. https://doi.org/10.14257/ijsip.2015.8.11.08

[8] Xu, X.J., Wang, Y.R., Chen, S. (2016). Medical image fusion using discrete fractional wavelet transform. Biomedical Signal Processing and Control, 27: 103-111. https://doi.org/10.1016/j.bspc.2016.02.008

[9] Karthikeyan, C., Ramadoss, B. (2016). Comparative analysis of similarity measure performance for multimodality image fusion using DTCWT and SOFM with various medical image fusion techniques. Indian Journal of Science and Technology, 9(22): 1-6. https://doi.org/10.17485/ijst/2016/v9i22/95298

[10] Chavan, S.S., Pawar, A., Talbar, S.N., Desai, S., Thakur, M., D'cruz, A. (2017). Non-subsampled rotated complex wavelet transform (NSRCxWT) for medical image fusion related to clinical aspects in neurocysticercosis. Computers in Biology and Medicine, 81: 64-78. https://doi.org/10.1016/j.compbiomed.2016.12.006

[11] Hill, P., Al-Mualla, M.E., Bull, D. (2017). Perceptual image fusion using wavelets. IEEE Transactions on Image Processing, 26(3): 1076-1088. https://doi.org/10.1109/tip.2016.2633863

[12] El-Hoseny, H.M., El-Rabaie, E.S.M., Elrahman, W.A., El-Samie, F.E.A. (2017). Medical image fusion techniques based on combined discrete transform domains. In 2017 34th National Radio Science Conference (NRSC), Alexandria, Egypt, pp. 471-480. https://doi.org/10.1109/nrsc.2017.7893518

[13] Udhaya Suriya, T.S., Rangarajan, P. (2017). Brain tumour detection using discrete wavelet transform based medical image fusion. Biomedical Research, 28(2): 684-688.

[14] Kaur, G., Singh, S., Vig, R. (2020). Medical fusion framework using discrete fractional wavelets and non-subsampled directional filter banks. IET Image Processing, 14(4): 658-667. https://doi.org/10.1049/iet-ipr.2019.0948

[15] Bhateja, V., Patel, H., Krishn, A., Sahu, A., Lay-Ekuakille, A. (2015). Multimodal medical image sensor fusion framework using cascade of wavelet and contourlet transform domains. IEEE Sensors Journal, 15(12): 6783-6790. https://doi.org/10.1109/jsen.2015.2465935

[16] Gomathi, P.S., Kalaavathi, B. (2016). Multimodal medical image fusion in non-subsampled contourlet transform domain. Circuits and Systems, 7(8): 1598-1610. https://doi.org/10.4236/cs.2016.78139

[17] Moin, A., Bhateja, V., Srivastava, A. (2016). Weighted-PCA based multimodal medical image fusion in contourlet domain. In Proceedings of the International Conference Information and Communication Technology. Advances in Intelligent Systems and Computing, pp. 597-606. https://doi.org/10.1007/978-981-10-0755-2_63

[18] Luo, X.Q., Zhang, Z.C., Zhang, B.C., Wu, X.J. (2017). Contextual information driven multi-modal medical image fusion. IETE Technical Review, 34(6): 598-611. https://doi.org/10.1080/02564602.2016.1228484

[19] Mehta, N., Budhiraja, S. (2018). Multimodal medical image fusion using guided filter in NSCT domain. Biomedical & Pharmacology Journal, 11(4): 1937-1946. https://doi.org/10.13005/bpj/1566

[20] Wang, K. (2019). Rock particle image fusion based on sparse representation and non-subsampled contourlet transform. Optik, 178: 513-523. https://doi.org/10.1016/j.ijleo.2018.09.121

[21] Rajalingam, B., Priya, R., Bhavani, R. (2020). Multimodal medical image fusion using Discrete Fractional Wavelet Transform (DFRWT) with Non-subsampled Contourlet Transform (NSCT) hybrid fusion algorithm. In New Trends in Computational Vision and Bio-inspired Computing, pp. 1131-1141. https://doi.org/10.1007/978-3-030-41862-5_115

[22] Rajalingam, B., Priya, R. (2018). Multimodal medical image fusion based on deep learning neural network for clinical treatment analysis. International Journal of ChemTech Research, 11(06): 160-176. https://doi.org/10.20902/ijctr.2018.110621

[23] Pei, C., Fan, K., Wang, W. (2020). Two-scale multimodal medical image fusion based on guided filtering and sparse representation. IEEE Access, 8: 140216-140233.

https://doi.org/10.1109/ACCESS.2020.3013027

[24] Li, S.T., Kang, X.D., Fang, L.Y., Hu, J.W., Yin, H.T. (2017). Pixel-level image fusion: A survey of the state of the art. Information Fusion, 33: 100-112. https://doi.org/10.1016/j.inffus.2016.05.004

[25] Liu, S.Q., Shi, M.Z., Zhu, Z.H., Zhao, J. (2017). Image fusion based on complex-shearlet domain with guided filtering. Multidimensional Systems & Signal Processing, 28: 207-224. https://doi.org/10.1007/s11045-015-0343-6

[26] Liu, X.B., Mei, W.B., Du, H.Q. (2017). Structure tensor and nonsubsampled shearlet transform based algorithm for CT and MRI image fusion. Neurocomputing, 235: 131-139. https://doi.org/10.1016/j.neucom.2017.01.006

[27] Du, J., Li, W.S., Lu, K., Xiao, B. (2016). An overview of multi-modal medical image fusion. Neurocomputing, 215: 3-20. https://doi.org/10.1016/j.neucom.2015.07.160

[28] Yang, Y., Que, Y., Huang, S.Y., Lin, P. (2017). Multiple visual features measurement with gradient domain guided filtering for multisensor image fusion. IEEE Transactions on Instrumentation and Measurement, 66(4): 691-703. https://doi.org/10.1109/TIM.2017.2658098

[29] Jian, L.H., Yang, X.M., Zhou, Z.L., Zhou, K., Liu, K. (2018). Multi-scale image fusion through rolling guidance filter. Future Generation Computer Systems, 83: 310-325. https://doi.org/10.1016/j.future.2018.01.039

[30] Zhu, J., Jin, W.Q., Li, L., Han, Z.H., Wang, X. (2018). Multiscale infrared and visible image fusion using gradient domain guided image filtering. Infrared Physics & Technology, 89: 8-19. https://doi.org/10.1016/j.infrared.2017.12.003

[31] Sreeja, P., Hariharan, S. (2018). An improved feature based image fusion technique for enhancement of liver lesions. Biocybernetics and Biomedical Engineering, 38(3): 611-623. https://doi.org/10.1016/j.bbe.2018.03.004

[32] Na, Y., Zhao, L., Yang, Y.X., Ren, M.Q. (2018). Guided filter-based images fusion algorithm for CT and MRI medical images. IET Image Processing, 12(1): 138-148. https://doi.org/10.1049/iet-ipr.2016.0920

[33] Meher, B., Agrawal, S., Panda, R., Abraham, A. (2019). A survey on region based image fusion methods. Information Fusion, 48: 119-132. https://doi.org/10.1016/j.inffus.2018.07.010

[34] Daniel, E. (2018). Optimum wavelet-based homomorphic medical image fusion using hybrid genetic–grey wolf optimization algorithm. IEEE Sensors Journal, 18(16): 6804-6811. https://doi.org/10.1109/JSEN.2018.2822712

[35] Daniel, E., Anitha, J., Kamaleshwaran, K.K., Rani, I. (2017). Optimum spectrum mask based medical image fusion using Gray Wolf Optimization. Biomedical Signal Processing and Control, 34: 36-43. https://doi.org/10.1016/j.bspc.2017.01.003

[36] El-Hoseny, H.M., El-Rahman, W.A., El-Rabaie, E.S.M., El-Samie, F.E.A., Faragallah, O.S. (2018). An efficient DT-CWT medical image fusion system based on modified central force optimization and histogram matching. Infrared Physics & Technology, 94: 223-231. https://doi.org/10.1016/j.infrared.2018.09.003

[37] Singh, N., Singh, S.B. (2017). Hybrid algorithm of particle swarm optimization and grey wolf optimizer for improving convergence performance. Journal of Applied Mathematics, 2017(1): 2030489. https://doi.org/10.1155/2017/2030489